N95- 21044

39739

18[157]

Simulation of a turbulent flame in a channel

By G. Bruneaux[1], K. Akselvoll[2], T. Poinsot[3] AND J. H. Ferziger[2]

The interaction between turbulent premixed flames and channel walls is studied. Combustion is represented by a simple irreversible reaction with a large activation temperature. Feedback to the flowfield is suppressed by invoking a constant density assumption. The effect of wall distance on local and global flame structure is investigated. Quenching distances and maximum wall heat fluxes computed in laminar cases are compared to DNS results. It is found that quenching distances decrease and maximum heat fluxes increase relative to laminar flame values. It is shown that these effects are due to large coherent structures which push flame elements towards the wall. The effect of wall strain is studied in flame-wall interaction in a stagnation line flow; this is used to explain the DNS results. It is also shown that 'remarkable' flame events are produced by interaction with a horseshoe vortex: burnt gases are pushed towards the wall at high speed and induce quenching and high wall heat fluxes while fresh gases are expelled from the wall region and form finger-like structures. Effects of the wall on flame surface density are investigated, and a simple model for flame-wall interaction is proposed; its predictions compare well with the DNS results.

1. Introduction

The interaction of a turbulent premixed flame with a wall is quite complex. First the flame is strongly influenced by the presence of the wall; which limits flame wrinkling and may cause the flame front to quench. Moreover, the flame has a significant effect on the flow in the vicinity of the wall: viscosity is greatly increased in the burnt gases, inhibiting turbulence. At the same time, flame elements approaching the wall increase the heat flux to as much as 1 MW/m² in practical situations. For these reasons, modeling flame–wall interactions in turbulent flows is an important issue (Amsden *et al.* 1985, Clendening *et al.* 1981, Lu *et al.* 1990). Models which try to predict these phenomena are available (Jennings 1992, Poinsot *et al.* 1993). However, little fundamental information is available so model building is a difficult exercise. An additional problem is that experiments are difficult to perform because the interesting phenomena occur very close to walls (typically less than 1 mm).

Our objective is to explore the flame-wall interaction mechanisms using three-dimensional direct numerical simulation (DNS). Two-dimensional variable-density simulations were performed in 1992 (Poinsot and Haworth, 1992) and led to a model

1 Institut Francais du Petrole, France and CTR, Stanford University

2 Stanford University

3 Institut de Mecanique des Fluides de Toulouse and CERFACS, France

used in piston engines (Poinsot *et al.* 1993). One of the main difficulties was the lack of a statistically stationary turbulent flow field. In the present study, a constant density turbulent channel flow was used. This has advantages and drawbacks: (1) the turbulence characteristics in the channel flow are well known and stationary which allows easy computation and (2), a constant density approximation has to be used, prohibiting feedback of the flame effects to the flow. However, this is a cost-effective approach.

2. Numerical method and configuration

In this study we extended the three dimensional DNS channel flow code written by Akselvoll & Moin (1993) to take reaction into account. Temperature and fuel mass fraction are treated as passive scalars and do not affect the flow. The flow solver has not been modified and is independent of the solver for the chemical species.

2.1 Basic equations

The flow solver solves the Navier-Stokes equations for an incompressible, constant viscosity flow:

$$\frac{\partial \widetilde{\rho}\widetilde{u}_i}{\partial \widetilde{t}} = -\frac{\partial \widetilde{p}}{\partial \widetilde{x}_i} - \frac{\partial \widetilde{\rho}}{\partial \widetilde{x}_j}\frac{\widetilde{u}_j\widetilde{u}_i}{} + \mu \frac{\partial^2 \widetilde{u}_i}{\partial \widetilde{x}_j^2} \tag{1}$$

$$\frac{\partial \widetilde{u}_i}{\partial \widetilde{x}_i} = 0 \tag{2}$$

The reaction solver solves the energy and species conservation equations, which allow convection, diffusion, and reaction effects:

$$\frac{\partial \widetilde{\rho}c_p\widetilde{T}}{\partial \widetilde{t}} + \frac{\partial \widetilde{\rho}c_p\widetilde{u}_i\widetilde{T}}{\partial \widetilde{x}_i} = \frac{\partial}{\partial \widetilde{x}_i}\left(\lambda \frac{\partial \widetilde{T}}{\partial \widetilde{x}_i}\right) + c_p(\widetilde{T}_2 - \widetilde{T}_1)\widetilde{\dot{w}}_R \tag{3}$$

$$\frac{\partial \widetilde{\rho}\widetilde{Y}_F}{\partial \widetilde{t}} + \frac{\partial \widetilde{\rho}\widetilde{u}_i\widetilde{Y}_F}{\partial \widetilde{x}_i} = \frac{\partial}{\partial \widetilde{x}_i}\left(\widetilde{\rho}D \frac{\partial \widetilde{Y}_F}{\partial \widetilde{x}_i}\right) - \widetilde{\dot{w}}_R \tag{4}$$

The superscript ($\sim$) refers to physical variables; absence of a superscript indicates a dimensionless variable.

We assume that $\widetilde{\rho}D = \widetilde{\rho}D_1 D^*$ where $D^* = (\widetilde{T}/\widetilde{T}_1)^b$ and $\lambda = \lambda_1\lambda^*$ where $\lambda^* = D^*$. The subscript 1 refers to the fresh gases, and the subscript 2 refers to the burnt gases.

The reaction is represented by a simple one-step mechanism, corresponding, for example, to lean combustion in which fuel is the limiting factor in determining the reaction rate (Williams, 1985). The reaction rate is expressed as:

$$\widetilde{\dot{w}}_R = \widetilde{\rho}\,\widetilde{Y}_F B\,exp\left(-\frac{\widetilde{T}_a}{\widetilde{T}}\right) \tag{5}$$

where B is the pre-exponential factor and $\widetilde{T}_a$ is the activation temperature.

The equations are nondimensionalized using the following dimensional quantities: $\tilde{u}_r$, the friction velocity at the wall, $\tilde{h}$, the channel half width, $\tilde{T}_1$, the temperature in the fresh gases, $\tilde{T}_2$, the temperature in the hot gases, $\tilde{Y}_1$, the fuel mass fraction in the fresh gases.

Physical and dimensionless variables are related in the following way:

$$\tilde{u} = \tilde{u}_r u, \quad \tilde{t} = \tilde{h}t/\tilde{u}_r, \quad \tilde{p} = \tilde{\rho}\tilde{u}_r^2 p, \quad \tilde{x} = \tilde{h}x, \quad T = \left(\tilde{T} - \tilde{T}_1\right)/\left(\tilde{T}_2 - \tilde{T}_1\right), \quad \tilde{Y}_F = \tilde{Y}_1 Y_F$$

giving the set of dimensionless equations:

$$\frac{\partial u_i}{\partial t} = -\frac{\partial p}{\partial x_i} - \frac{\partial u_j u_i}{\partial x_j} + \frac{1}{Re}\frac{\partial^2 u_i}{\partial x_j^2} \tag{6}$$

$$\frac{\partial u_i}{\partial x_i} = 0 \tag{7}$$

$$\frac{\partial T}{\partial t} + \frac{\partial u_i T}{\partial x_i} = \frac{1}{RePr}\frac{\partial}{\partial x_i}\left(\lambda^* \frac{\partial T}{\partial x_i}\right) + \dot{w}_R \tag{8}$$

$$\frac{\partial Y_F}{\partial t} + \frac{\partial u_i Y_F}{\partial x_i} = \frac{1}{RePrLe}\frac{\partial}{\partial x_i}\left(D^* \frac{\partial Y_F}{\partial x_i}\right) - \dot{w}_R \tag{9}$$

where the Reynolds number is $Re = \frac{\tilde{\rho}\tilde{u}_r\tilde{h}}{\tilde{\mu}}$, the Prandtl number is $Pr = \frac{\tilde{\mu}c_p}{\tilde{\lambda}_1}$, and the Lewis number is $Le = \frac{\tilde{\lambda}_1}{\tilde{\rho}c_p\tilde{D}_1}$. The reaction rate expression can be reduced to (Williams, 1985):

$$\dot{w}_R = Da Y_F exp\left(-\frac{\beta(1-T)}{1-\alpha(1-T)}\right) \tag{10}$$

where α is the temperature factor $\alpha = (\tilde{T}_2 - \tilde{T}_1)/\tilde{T}_2$, β is the reduced activation energy $\beta = \alpha\tilde{T}_a/\tilde{T}_2$, and Da is the reduced pre-exponential factor $Da = \frac{B\tilde{h}}{\tilde{u}_r}exp\left(-\frac{\beta}{\alpha}\right)$.

2.2 Numerical implementation

These equations are solved in a Cartesian coordinate system using a second-order finite difference scheme. All terms are treated explicitly except the diffusive terms in the wall-normal direction in the momentum equation, which are treated implicitly. The time discretization is second-order Adams-Bashforth for the explicit terms and second order Crank-Nicolson for the implicit terms. The pressure is used to correct the velocity field so that it satisfies the continuity equation; this requires a Poisson solver.

The flow and flame structure are computed on different meshes. The mesh spacing for the flow needs to be small enough near the wall to resolve the viscous sublayer, typically $\Delta y^+ = 0.1$, but in the center of the channel, $\Delta y^+ = 8$ is sufficient (Kim *et al.* 1987); here the superscript ($^+$) denotes wall units. Because the structure of the turbulence is elongated in the streamwise direction, $\Delta x^+ = 35$ and $\Delta z^+ = 5$. The mesh distribution along the y axis is given by $y_j = \left(1 - \frac{\tanh\left(a\frac{Y_L}{2}(1-(j-1)/(NY-1))\right)}{\tanh\left(a\frac{Y_L}{2}\right)}\right)\frac{Y_L}{2}$ where a is a stretching parameter. Large

values of a distribute more points near the wall. NY is the number of points and Y_L is the size of the box in the y direction.

The flame computation is best done on a uniform mesh in all directions in order to resolve the flame equally well everywhere in the computational domain.

For this reason, different meshes are used in the computation, one for the velocity and pressure, and another for the temperature and fuel mass fraction. The velocities are interpolated from the flow mesh to the reaction mesh. Three-dimensional linear interpolation based on data at the eight corners of the smallest box (of the flow mesh) surrounding the reaction grid point is used. This interpolation procedure was tested by running laminar flame-wall interaction cases in two dimensions and does not introduce additional error because the velocity grid near the wall is much denser than the temperature grid.

2.3 Initial and boundary conditions

The walls are no-slip and isothermal. The flow, temperature and mass fraction fields are periodic in the x and z directions.

The initial conditions for the flow are obtained by running the flow solver until stabilized (in the statistical sense) values of the velocities and pressure are obtained. The temperature and mass fraction are introduced at $t = 0$ as two back-to-back one-dimensional laminar flames propagating towards the walls.

3. Code validation and computation of reference flows

3.1 Computation of non-reacting turbulent channel flow

A first calculation was made without a flame to validate the flow solver. The flow field is initialized from a random field, and is run until the values of velocities and pressure stabilize. Mean quantities are calculated by averaging in the x and z directions and time.

The configuration is the minimal channel flow with $Re = 180$, and uses a stretching factor $a = 2.9$. The dimensions of the domain are $X_L = 3.14159$, $Y_L = 2.$, and $Z_L = 0.908$, with $NX = 18$, $NY = 130$ and $NZ = 34$. The results are consistent with well-known results of channel calculations (Kim *et al.* 1987). Fig. 1 shows the mean velocity profile along with the log law, and Fig. 2 shows the profiles of turbulent velocity components compared to the results of Kim *et al.* 1987. The discrepancies are due to the fact that we have performed a minimal channel simulation while Kim *et al.* did a full channel simulation.

3.2 Quenching of laminar flames on walls in stagnant flow

One-dimensional calculations were performed to validate the reaction solver. The temperature profile of a constant viscosity flame is calculated using an analytical-numerical approach (Rutland 1989). Then this profile is used as an initial condition to compute a flame having variable transport properties with the reaction code, in which the flame is stabilized by prescribing a uniform inlet velocity equal to the flame speed. The temperature profile obtained is then used to initialize the flame-wall interaction calculation (laminar or turbulent).
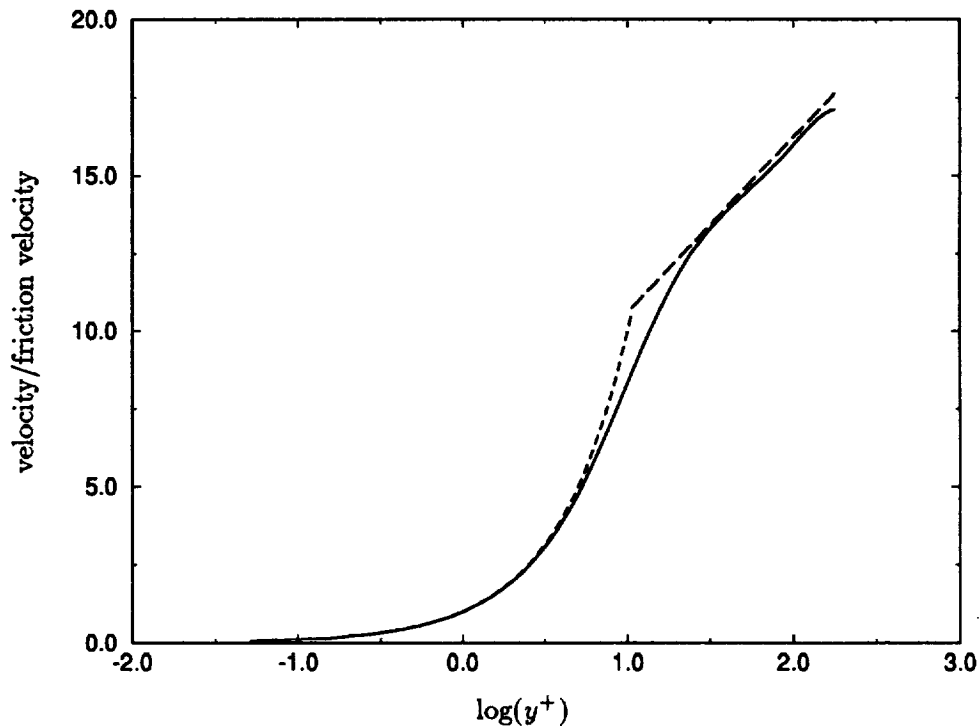
FIGURE 1.   Profiles of mean velocity compared to the laminar and log laws.
——— linear law, ——— log law, ——— mean velocity.

We first performed a one-dimensional calculation corresponding to head-on quenching in stagnant fluid. The flame propagates normal to the wall, fresh gases are trapped between the flame and the wall, and the fluid velocity is zero everywhere. The flame consumes reactant as it moves towards the wall. When the flame-wall distance δ reaches its minimum, the wall heat flux Φ is maximum; the consumption rate s_c decreases to zero exponentially thereafter, as shown in Fig. 3. The phenomena occurring in this interaction have been discussed previously (Adamczyk and Lavoie 1978, Carrier *et al.* 1979, Wichman and Bruneaux 1994). The flame-wall distance is non-dimensionalized by a typical flame thickness $d = \lambda/(\tilde{\rho}c_p s_l^0)$ to form a Peclet number $Pe = \delta/d$ and the wall heat flux is non-dimensionalized by the flame power $P = \tilde{\rho}c_p s_l^0(\tilde{T}_2 - \tilde{T}_1)$ to produce a reduced heat flux $\phi = \Phi/P$. At quenching the minimum Peclet number is $Pe = 3.68$ and the maximum reduced wall heat flux is $\phi = 0.56$. These values are different from the previous results of Poinsot *et al.* (1993) because the assumptions are different; in particular, they allowed variable density and had a different Prandtl number ($Pr = 0.75$).
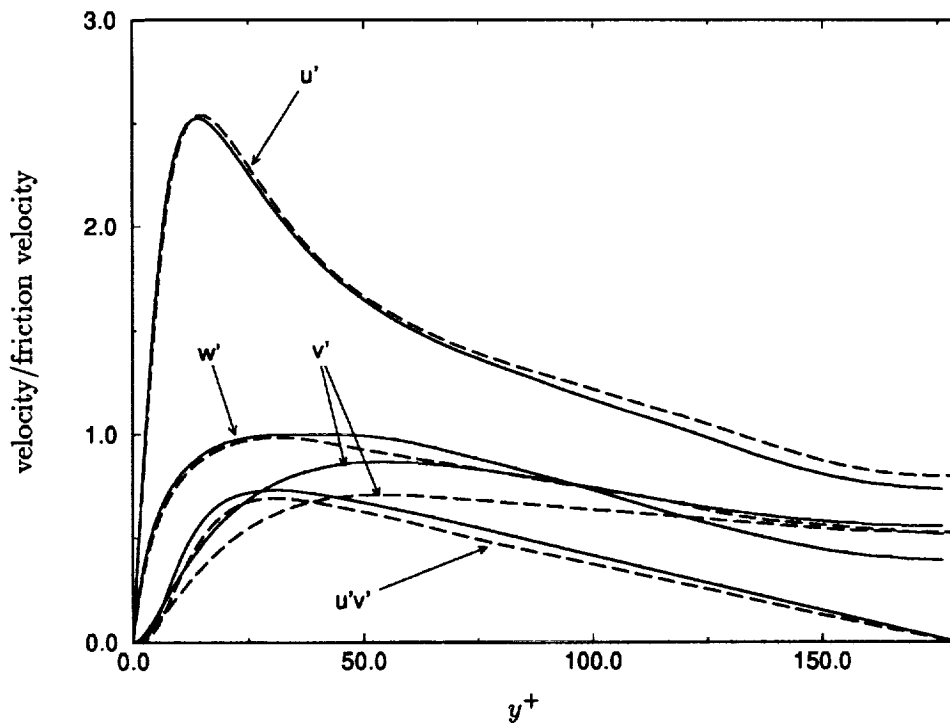
FIGURE 2.   Profiles of fluctuating velocities. ——— DNS minimum channel,
——— Kim *et al* 1987.

Table I. Fixed parameters for DNS of turbulent channel.

Re	Le	Pr	b	α	β	Da	s_l^0/u_τ	δ_l^0/h	δ_l^0/d
180.	1.	0.5	1.	0.75	6.	80.4	0.36	0.15	5.0

We investigated the influence of grid resolution on the laminar flame speed (mass consumption rate) for a stabilized flame and on the maximum wall heat flux during flame-wall interaction. The results are shown in Fig. 4. For the maximum wall heat flux we also compared first and second order treatment of the wall boundary condition $\left(\frac{\partial Y_F}{\partial y}\right)_{wall} = 0$. The results show that 65 points in the half-channel and a second order scheme at the wall suffice.

3.3 Quenching of laminar flames on walls in stagnation line flow

We also performed one-dimensional calculation of flame interacting with a wall in a stagnation line flow. A flow field corresponding to a stagnation line flow with $\frac{\partial v}{\partial y} = -\Gamma$; Γ, the strain rate is non-dimensionalized by the inverse characteristic
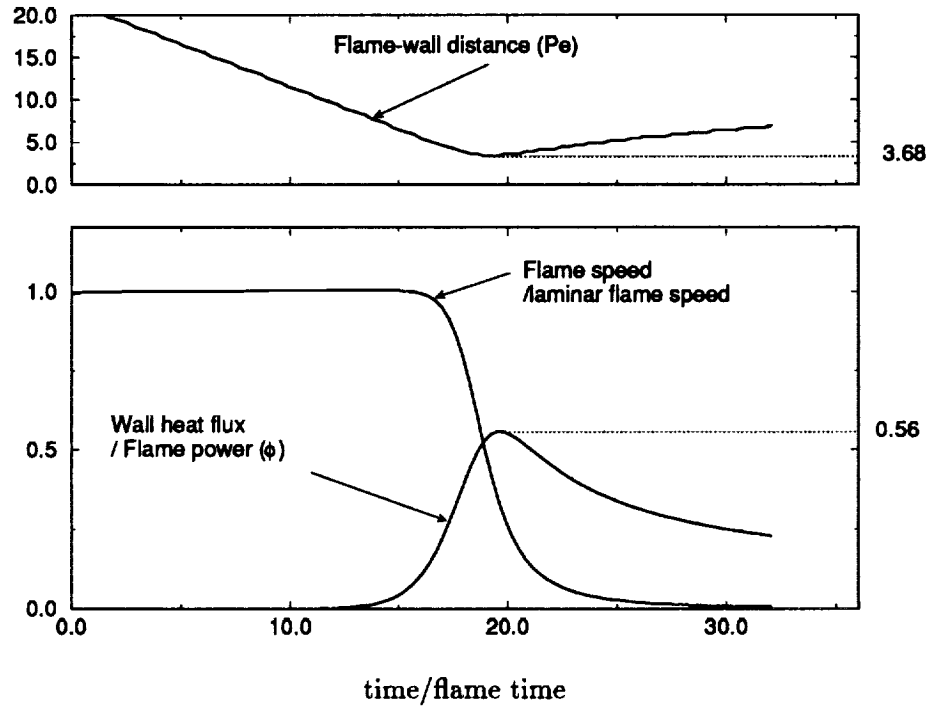
FIGURE 3. Time evolution of wall heat flux, flame speed (consumption rate), and flame-wall distance for a laminar flame-wall interaction in a stagnant flow.

flame time scale s_l^0/δ_l^0 to produce a reduced strain rate $\gamma = \Gamma/(s_l^0/\delta_l^0)$. A typical result for strained flame-wall interaction is presented in Fig. 5, for $\gamma = 5$. At first, the flame adjusts to the flow and the flame speed decreases to a stable value. Then the flame begins to interact with the wall. Because the flame is convected towards the wall, the interaction is faster than in the stagnant flow and produces a higher maximum wall heat flux and a smaller minimum flame wall-distance. In the stagnant case, the interaction lasts about 6 flame times, while for a strained flame with $\gamma = 1$, it lasts 3.5 flame times, and for $\gamma = 5$, 3 flame times. Fig. 6 shows the effect of the strain rate γ on the maximum wall heat flux ϕ and on the minimum flame-wall distance Pe.

4. Results for turbulent flame wall interaction

4.1 Evolution of global quantities during interaction

Fig. 7 presents the evolution of the mean fuel mass fraction, the turbulent flame speed, and the total turbulent flame surface for a typical periodic run together with the laminar values. The parameters are those of the non-reacting flow and the laminar flame.

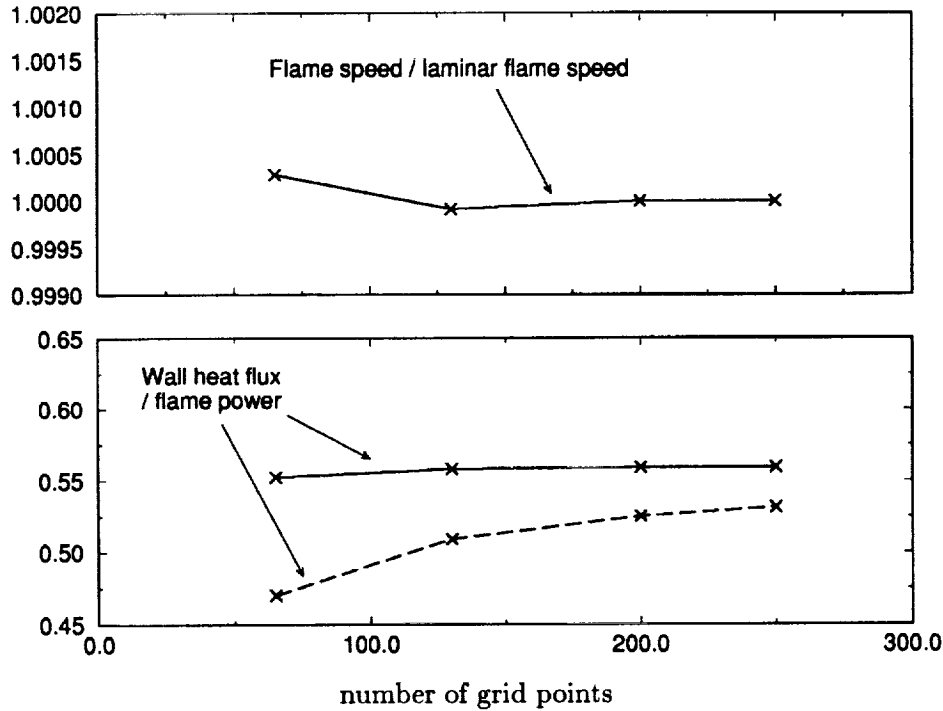Early in the simulation, the flames are not yet wrinkled and are located near

FIGURE 4.   Influence of grid resolution and order of accuracy on laminar flame speed and maximum wall heat flux. × —————— × first order, × —————— × second order.

the center of the channel where the turbulence is weak. After $t/t_f > 3$ where $t_f = d/s_l = \lambda_1/\rho c_p(s_l^0)^2$, d is a typical flame thickness and s_l^0, the laminar flame speed, wrinkling increases as does the consumption rate of reactants, producing a maximum turbulent flame speed 1.5 times the laminar flame speed. Then, at $t/t_f = 10$, the flames begin to interact with the walls and the consumption rate is reduced due to lack of reactants. The turbulent flame speed is never constant.

Fig. 8 presents the surface with $T = .85$ and the reaction rate in the turbulent flame at $t/t_f = 9$. Quenching is observed, and a finger-like structure is also present. The mechanism of formation of this structure will be explained below.

4.2 A correlation between local wall strain rate and flame quenching

For practical applications the most important quantity is the maximum wall heat flux. Fig. 9 displays the variations of the minimum flame wall distance and the maximum wall heat flux (normalized by laminar quantities) with time. Fig. 9 also displays the effect of grid resolution on these quantities: a second calculation was performed with twice the number of points in the y direction. No effect of grid resolution is seen. Clearly, the turbulent flame comes closer to the wall and produces higher heat fluxes than the unstrained laminar flame. This differs from results obtained previously and appears to be due to the structure of the turbulence.
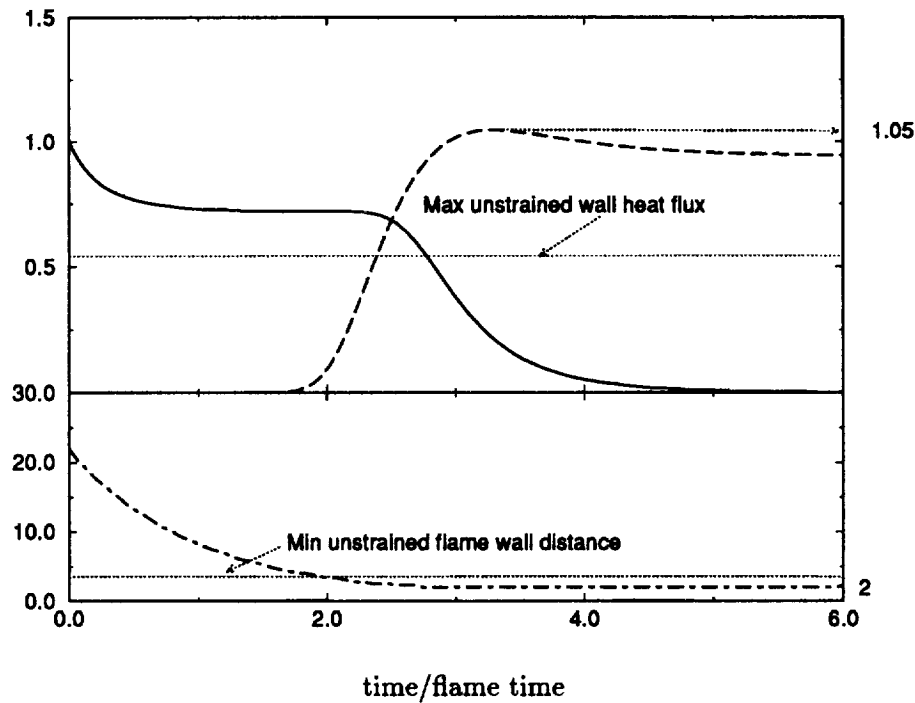
FIGURE 5. Time evolution of wall heat flux, flame speed and flame-wall distance in a laminar flame-wall interaction in a stagnation line flow with $\gamma = 5$. ——— flame speed/laminar flame speed, — — — wall heat flux/flame power (ϕ), — · — · flame-wall distance (Pe).

In the simulations of Poinsot *et al.* (1993), the turbulence was two-dimensional so there was no small scale structure near the walls. In the present case, the typical quenching distance δ_Q is larger than the viscous sublayer thickness (typically $\delta_Q^+ \simeq 28$) and turbulent structures modify the structure of the flame near the wall.

Another way of presenting this phenomenon is to look at trajectories in a (Peclet number–heat flux) diagram. Fig. 10 presents such trajectories for the laminar flame, for the turbulent flame at $t/t_f = 7.3$, and for two strained laminar flames. The envelop of the turbulent results lie close to the trajectory of the laminar strained flame with $\gamma = 5$, indicating that the effect is primarily due to the strain. This was further checked by computing the strain rate statistics shown in Fig. 11. Because the strain rate is not constant in the turbulent case, we plotted the normal component of the velocity at the flame location divided by the flame-wall distance. We will see in the next section how these large strain rates are created.

4.3 The importance of flow structures

Near-wall coherent structures have a strong effect on the flame. In the case presented here, we find the interaction of a horseshoe vortex with the flame is quite
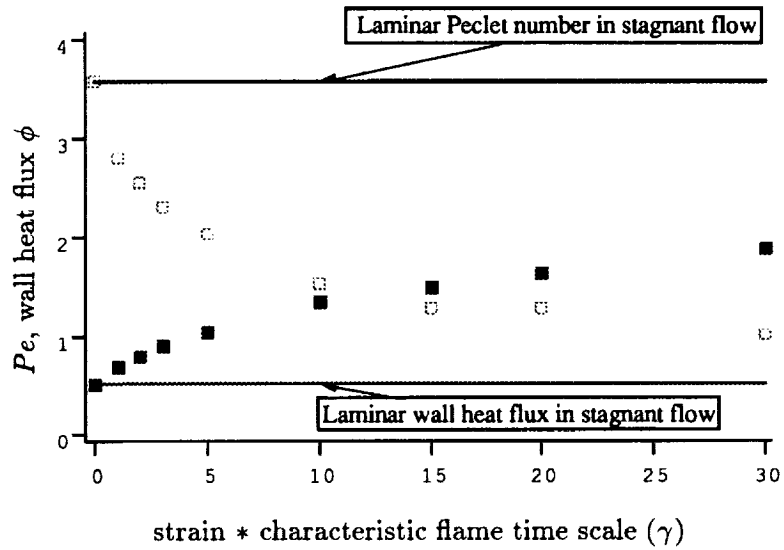
FIGURE 6.   Effects of wall normal strain γ on flame-wall quenching of laminar flames. ■ wall heat flux/flame power (ϕ), □ flame wall distance (Pe).
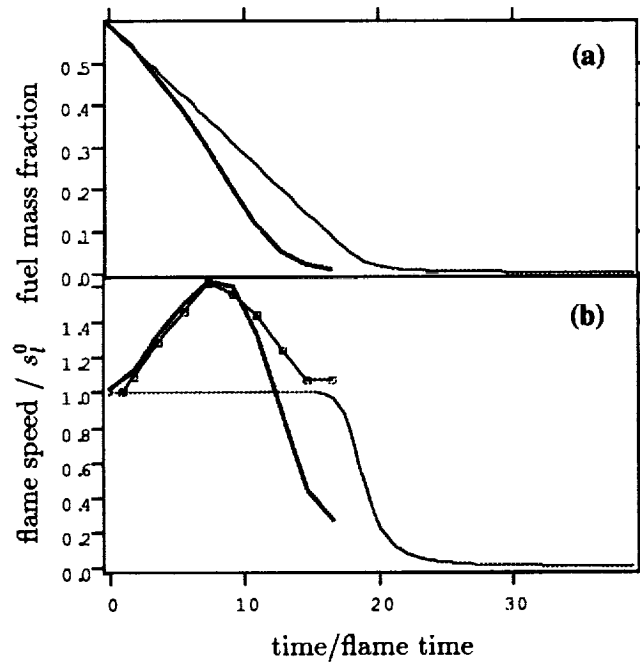

FIGURE 7.   Evolution of global quantities during turbulent flame wall interaction. (a) —— laminar, —— turbulent, (b) —— laminar flame speed, —— turbulent flame speed, -□- total flame surface/initial flame surface.
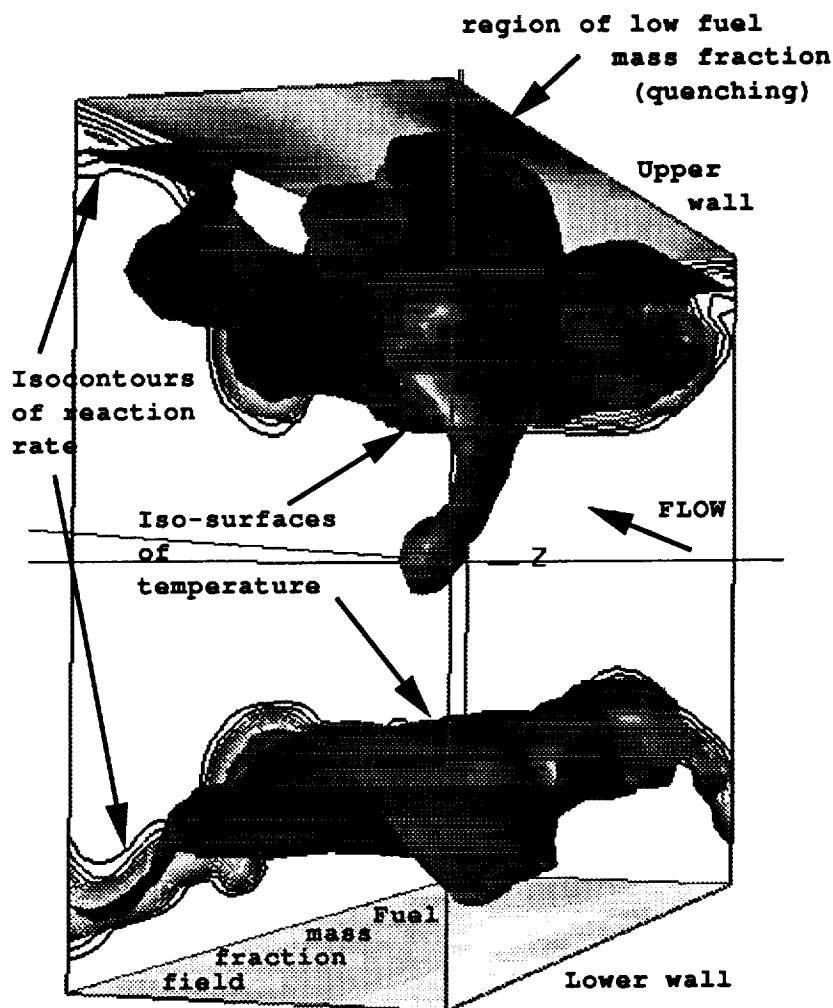
FIGURE 8. Snapshot of isosurface of temperature $T = 0.85$, along with reaction rate isolines and fuel mass fraction field, $t/t_f = 9$.

important. It produces the following events:

(1) The horseshoe vortex pushes burnt gases towards the wall and leads to flame quenching with small Peclet number and large heat flux.

(2) At the same time, the other side of the horseshoe vortex pushes fresh gas away from the wall, leading to the formation of an unburnt gas tongue; tongues similar to this one have been seen in experiments.

Fig. 12 shows an instantaneous picture of a one-legged horseshoe vortex wrapping a flame and leading to quenching at the wall and ejection of fresh gas.
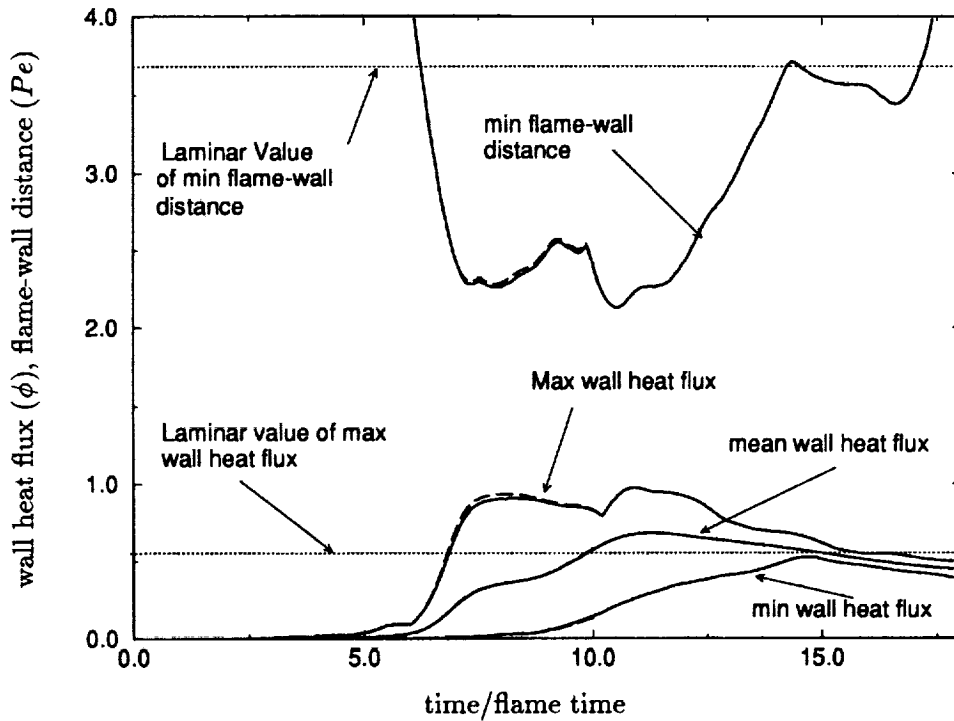
FIGURE 9.   Time evolution of minimum flame-wall distance, minimum, mean, and maximum wall heat flux in the turbulent calculation. Comparison with a higher resolution calculation is also shown. ———— $NY = 130$, ———— $NY = 260$.

5. A model for the quenched interface density

5.1 Mean quantities

Since periodic boundary conditions were used, averaging may be performed in the two directions parallel to the wall (x and z) at each instant. Quantities computed using conventional averaging include the mean fuel mass fraction $\overline{Y}_F$, the mean temperature $\overline{T}$, and the mean reaction rate $\overline{\omega}$. It is convenient to replace the mean reaction rate $\overline{\omega}$ by an equivalent reactive flame surface density $\overline{\Sigma}_R$ defined by $\overline{\Sigma}_R = \overline{\omega}/s_l^0$. Profiles of these quantities are plotted in Fig. 13.

We also estimated the density $\overline{\Sigma} = \langle \Sigma' \rangle$ of interface between fresh and burnt gases. Σ' is the local surface to volume ratio, calculated where the surface (defined as the isosurface with reduced temperature 0.85) is approximated using the angle between the local temperature gradient and a coordinate direction (Rutland 1989). In the absence of quenching or strain, $\overline{\Sigma}$ is related to $\overline{\omega}$ by $\overline{\omega} = \overline{\Sigma} s_l^0$ or $\overline{\Sigma}_R = \overline{\Sigma}$ (we used Lewis number unity for this flame. Near the wall, part of this interface is quenched so $\overline{\omega} < \overline{\Sigma} s_l^0$. We will characterize quenching by the quenched fraction defined by $Q = \frac{\overline{\Sigma} - \overline{\Sigma}_R}{\overline{\Sigma}}$.

Early in the simulation ($t/t_f = 1.8$, Fig. 13), the flame is far from the wall, no

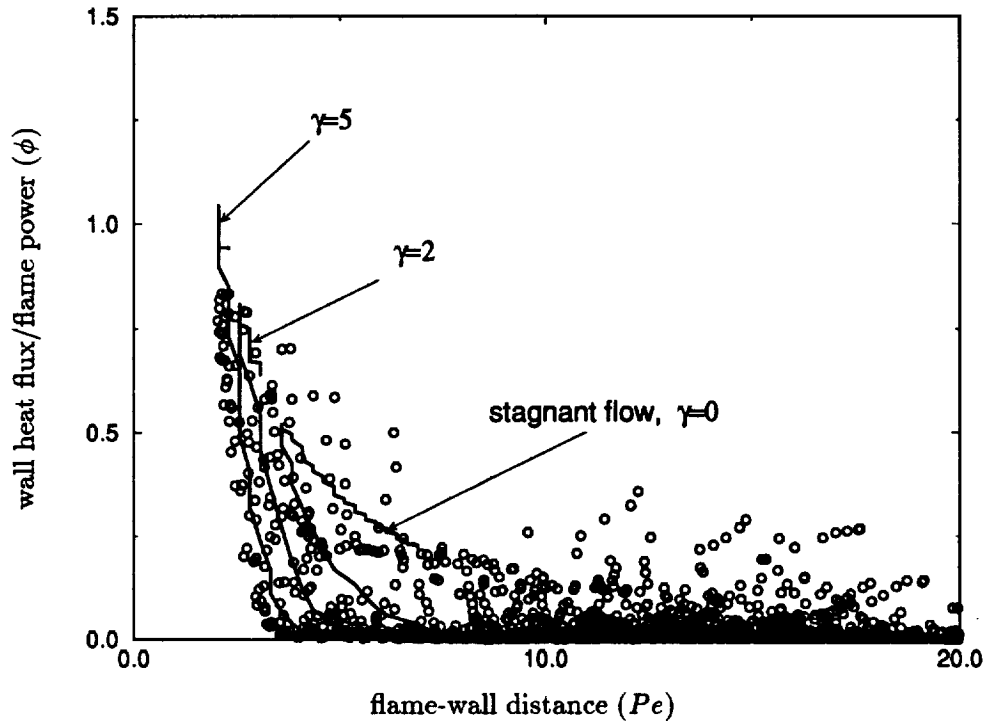FIGURE 10. Trajectory in the Pe-wall heat flux plane of the turbulent flame at $t/t_f = 7.3$, along with trajectories for laminar flame-wall interaction in stagnant flow and stagnation line flow. o turbulent $t/t_f = 7.3$, ——— laminar.

quenching takes place, and the profile of the interface density $\overline{\Sigma}$ matches the profile of the normalized reaction rate $\overline{\Sigma}_R$. The noise in Fig. 13 is due to the fact that $\overline{\Sigma}$ is computed by estimating surface area while the mean reaction rate $\overline{\omega}$ and the reactive interface density $\overline{\Sigma}_R$ are computed using conventional averages. The mean fuel mass fraction at the wall is still the initial value and the burnt gases occupy only a small fraction of the channel. The quenched fraction Q is zero everywhere; the wall heat flux is also essentially zero.

Later ($t/t_f = 12.8$, Fig. 13), the flame brush starts to interact with the wall and quenching takes place. This increases the interface density relative to the reactive interface density and thus the quenched fraction near the wall. The mean temperature gradient is not zero at the wall, indicating that the mean wall heat flux is no longer zero (see Fig. 9). In addition, the mean fuel mass fraction at the wall starts to decrease.

Finally ($t/t_f = 14.7$, Fig. 13), most of the fresh gases in the channel have been consumed and the interface density is much larger than the reactive surface density. Most of the interface is quenched. Very little fuel is available and the wall heat flux is large.
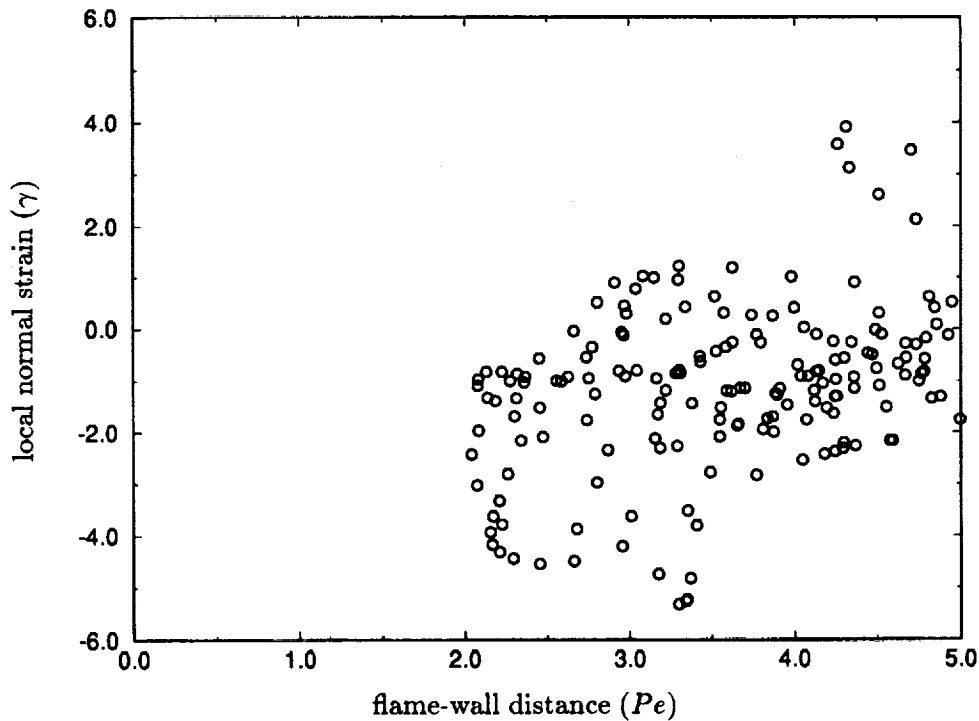
FIGURE 11.   Trajectories in Pe-(equivalent) normal wall strain rate diagram at $t/t_f = 7.3$.

5.2 A model for the quenched interface fraction

It is well known that interaction between flames and walls or, more generally, the behavior of non-adiabatic flames may be characterized in terms of enthalpy loss L_H (Williams 1985, Wichman and Bruneaux 1994) defined by

$$L_H = 1 - (Y_F + T)$$ (11)

In an adiabatic premixed flame with unity Lewis number, L_H is zero everywhere. When the flame is non-adiabatic (as near walls), L_H increases, which indicates that quenching is possible. This is true for turbulent flames if we assume that heat and species diffuse at the same rate (turbulent Lewis number equal to unity).

A simple model for the quenched interface fraction Q may be derived by assuming that Q is proportional to the enthalpy loss L_H times the interface density:

$$Q_{model} = L_H * \overline{\Sigma} * L_Q$$ (12)

where L_Q is a multiple of the laminar flame thickness δ_l^0. For the present, we assume $L_Q = 10\delta_l^0$.
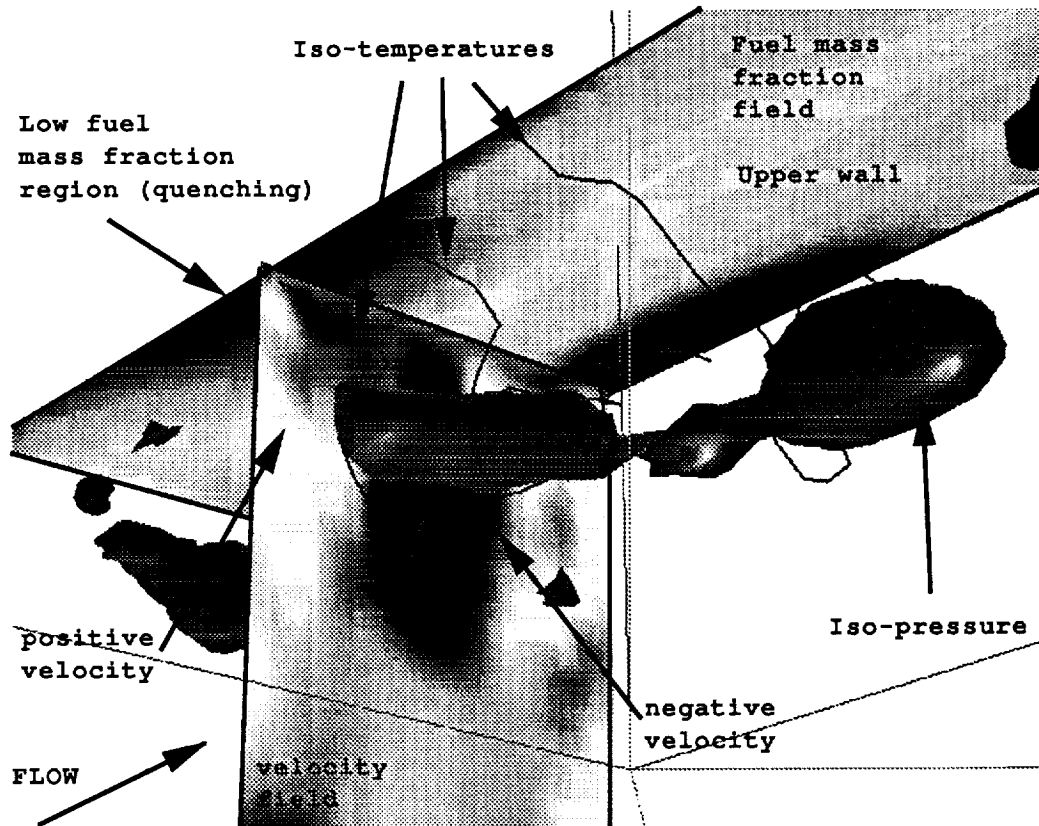
FIGURE 12. Snapshot of isosurface of low pressure (which marks a horseshoe vortex) together with the velocity and fuel mass fraction fields at $t/t_f = 7.3$.

Despite its simplicity, this model retains much of the physics of flame quenching: quenching occurs only where flame surface is present and the flame has lost significant enthalpy.

This model was tested against DNS results and the results are given in Fig. 14. The agreement between the modeled value Q_{model} and the DNS value Q is good. The model predicts both the spatial extent of the quenching as well as its magnitude. Only late in the simulation ($t/t_f = 14.7$, Fig. 14) does the model underpredict the extent of quenching and then only in the region far from the wall.

Conclusions

Direct numerical simulations of flame-wall interactions have been performed using a three-dimensional channel flow code and a constant density reaction solver. Non-reacting turbulent flow and laminar reaction in stagnant and stagnation line flow were used to validate the code. In turbulent flows the wall heat fluxes are much higher than in the laminar stagnant flame-wall interaction. This is due to the turbulence which convects flame elements towards the wall, inducing high heat fluxes
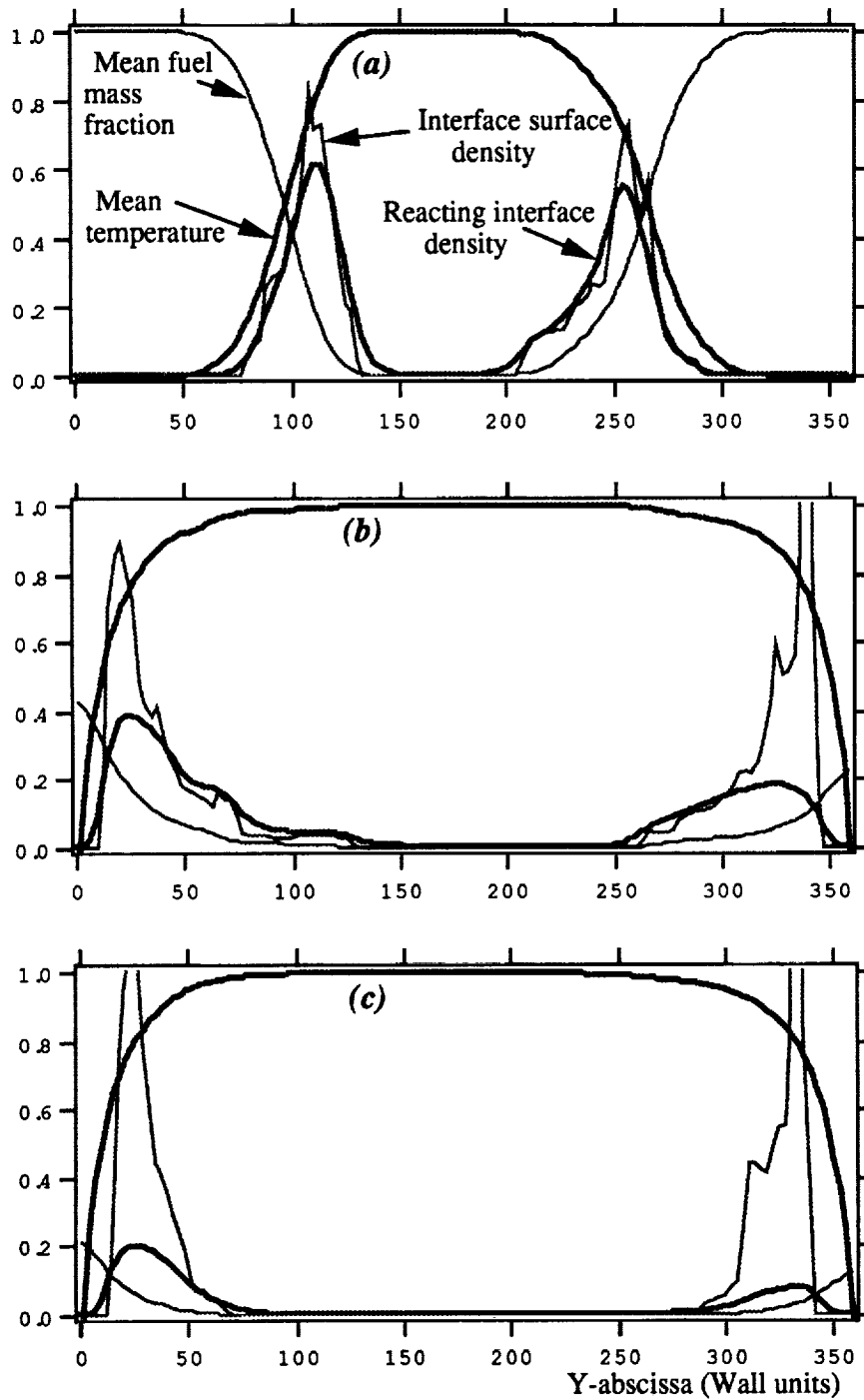
FIGURE 13.   Mean values of temperature, mean fuel mass fraction, reactive surface, and interface density. a): $t/tf = 1.8$; b): $t/tf = 12.8$; c): $t/tf = 14.7$.

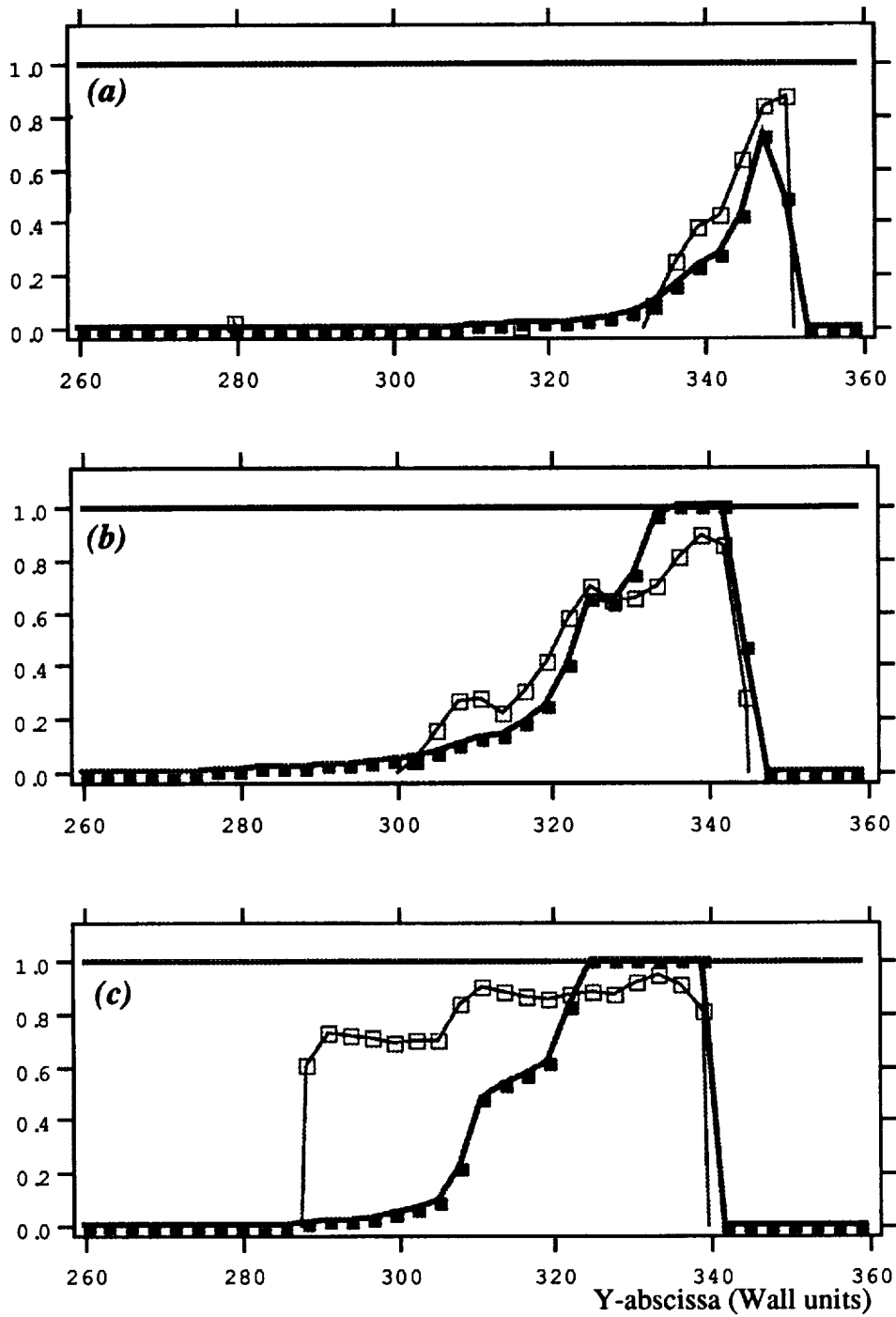FIGURE 14. Comparison between modeled and DNS-measured quenched fractions. -□- DNS mesured quenched fraction, -■- Model for quenched fraction. a): $t/tf = 9$; b): $t/tf = 12.8$; c) $t/tf = 14.7$.

to the wall. The turbulent flame was compared to a flame in a stagnation line flow, leading to the conclusion that high wall heat fluxes are due to high normal strain. In the turbulent case, the high normal strain is generated by horseshoe vortices which push flame elements towards the wall while fresh gases are convected away from the wall, forming finger-like structures. A model for the quenched fraction of interface was proposed and compares well to the DNS results, despite its simplicity.

REFERENCES

ADAMCZYK, A. A. & LAVOIE, G. A. 1978 Laminar head-on flame quenching: a theoretical study. *SAE Transactions 87, SAE Paper 780969.*

AKSELVOLL, K. & MOIN, P. 1993 Large eddy simulation of a backward facing step flow. *Engineering Turbulence Modeling and Experiments 2.* W. Rodi and F. Martelli eds., Elsevier, 303-313.

AMSDEN, A., RAMSHAW, J., O'ROURKE, P. & DUCKOWICZ, J. 1985 SAE Paper 850554.

CARRIER, G. F., FENDELL, F. E., BUSH, W. B., & FELDMAN, P. S. 1979 Nonisenthalpic interaction of a planar premixed laminar flame with a parallel end wall. *SAE Paper 790245.*

CLENDENING, J. C. W., SHACKLEFORD, W. & HILYARD, R. 1981 Raman scattering measurement in a side wall quench layer. *18th Symp. (Intl.) on Combust.* The Combustion Institute, Pittsburgh, 1583-1589.

JENNINGS, M. 1992 SAE Paper 920589.

KIM, J., MOIN, P., & MOSER, R. 1987 Turbulence statistics in fully developed channel flow at low Reynolds number. *J. Fluid Mech.* **177**, 133-166.

LU, J. H., EZENKOYE, O., GREIF, R. & SAWYER, R. F. 1990 Unsteady heat transfer during side wall quenching of a laminar flame. *23rd Symp. (Intl.) on Combust.* The Combustion Institute, Pittsburgh, 441-446.

POINSOT, T. J., & HAWORTH, D. C. 1992 Proceedings of the 1992 Summer Program. CTR, NASA Ames/Stanford University, Stanford.

POINSOT, T. J., HAWORTH, D. C., & BRUNEAUX, G. 1993 Direct simulation and modeling of flame-wall interaction for premixed turbulent combustion. *Combust. & Flame.* **95**, 118-132.

RUTLAND, C. 1989 Effects of strain, vorticity, and turbulence on premixed flame. Ph.D. Thesis, Stanford University, Stanford.

WICHMAN, I. S. & BRUNEAUX, G. 1994 Head-on quenching of a premixed flame by a cold wall. *submitted to Combust. & Flame.*

WILLIAMS, F. A. 1985 *Combustion theory.* B. Cummings, Menlo Park, CA, 73-76.